Mar Syst Ocean Technol (2017) 12:211–230
DOI 10.1007/s40868-017-0035-1

Floating breakwater concept for large LNG terminals: part 1. Parametric study and process design

F. Ruggeri[1] · R. A. Watai[1] · G. F. Rosetti[1] · R. S. Lavieri[1] · R. Dotta[2] · J. A. Ferrari Junior[3] · K. Nishimoto[2]

Received: 19 October 2016 / Accepted: 18 August 2017 / Published online: 5 September 2017

Abstract Part 1 of this two-part paper presents the development of a parametric model for the design of a floating breakwater conceived to protect a LNG terminal. The model is composed by a set of numerical scripts that perform the classical steps of a typical design spiral in order to evaluate weights and centers, stability margins, structural loads, wave attenuation capability, and seakeeping performance. Each of these models is discussed in terms of sensitivity analysis, which demonstrates the influences of different parameters in the global design. Especial attention is given to the analysis of the structure wave attenuation capability, in which the effects of water depth, underkeel clearance, wave period and direction, breakwater motions are investigated.

Keywords Floating breakwater · LNG terminals · Attenuation capability · Floating structures

1 Introduction

Breakwater types may be synthesized as mound type structures (ex: rubble-mound, precast units, sheet-steel modules etc.), monolithic types (ex: caisson units), composite types, and floating breakwaters (ex: pontoons), as illustrated in Fig. 1. Independently of their types, its main purpose is to protect harbors, moored vessels, and terminals from excessive incidence of sea waves.

✉ F. Ruggeri
felipe.ruggeri@gmail.com

[1] Argonáutica Engineering & Research, São Paulo, Brazil

[2] Numerical Offshore Tank (TPN) – University of São Paulo (USP), São Paulo, Brazil

[3] BG Group, Rio de Janeiro, Brazil

According to Fousert [4] and Biesheuvel [2], mound types of breakwaters consist of large heaps of rocks or concrete blocks, which are attractive to be applied only in shallow waters. In deeper waters, the costs for construction increase rapidly, since the structure requires an enormous amount of material. Monolithic breakwaters are large solid blocks, such as block walls and caissons. This type of breakwater structure is suitable to be used in medium water depths, since it becomes cheaper to be applied in comparison to a mound type one [2]. On the other hand, the soil conditions must be appropriate to enable a stable foundation of the heavy block elements.

Composite type of breakwater is understood as a combination of the mound and monolithic types of breakwater, being often preferred from an economical point of view when water depths are slightly increased. However, in deep water, bottom-founded breakwaters cannot be used and floating breakwaters are the only choice.

Differently from fixed types, the cost of a floating system is not significantly dependent on water depth and foundation conditions. Fousert [4] presented a comparison of construction costs depending on the water depths for the different concepts of breakwaters aforementioned, concluding that, for water depths larger than 30 m, the floating type would be the most feasible solution from an economical point of view (Fig. 2). Other advantages are that floating breakwaters have a minimal interference with water circulation, sediment transport, coral reef formations, and fish migration, thus being environmentally friendly solution [7].

Floating breakwaters also present some disadvantages which must be carefully evaluated. Hales [5] states that the design of floating breakwater systems must be carefully matched to the site conditions, especially concerning long waves which may arrive from infrequent storms. This is explained by the fact that floating breakwaters fail to meet

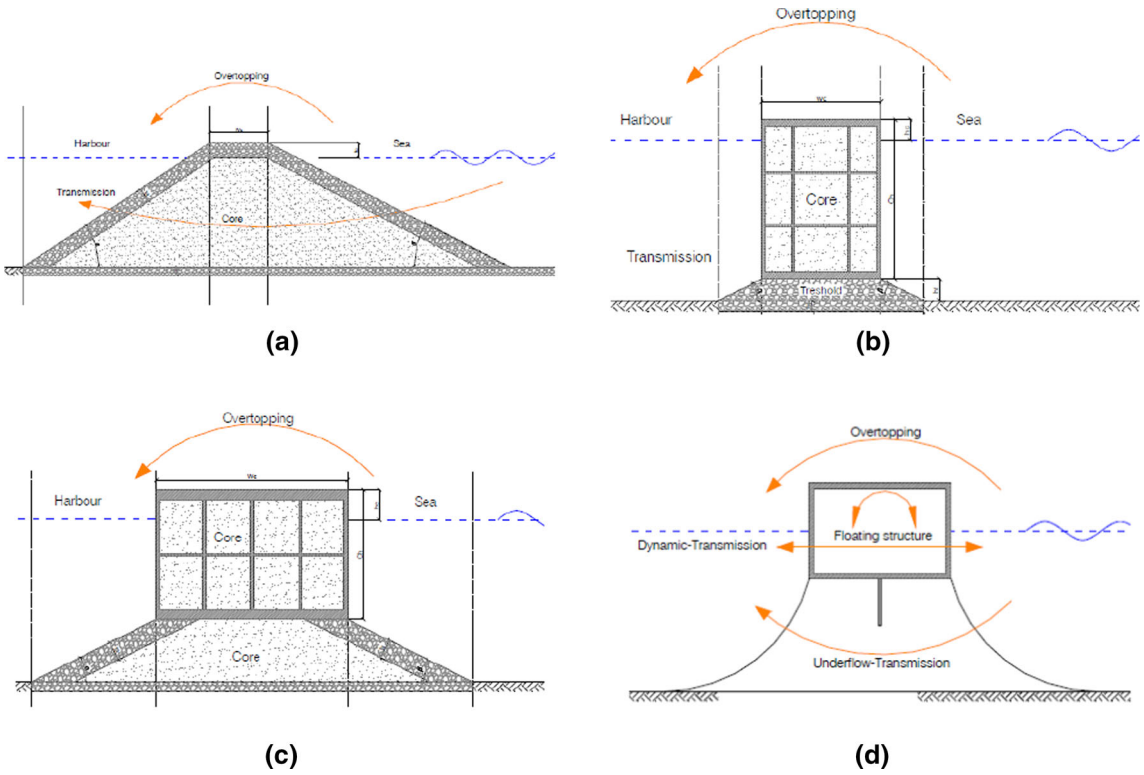

Fig. 1 Different breakwater structures. **a** Mound types, **b** monolithic types, **c** composite types, and **d** floating breakwaters. *Source* Fousert [4]

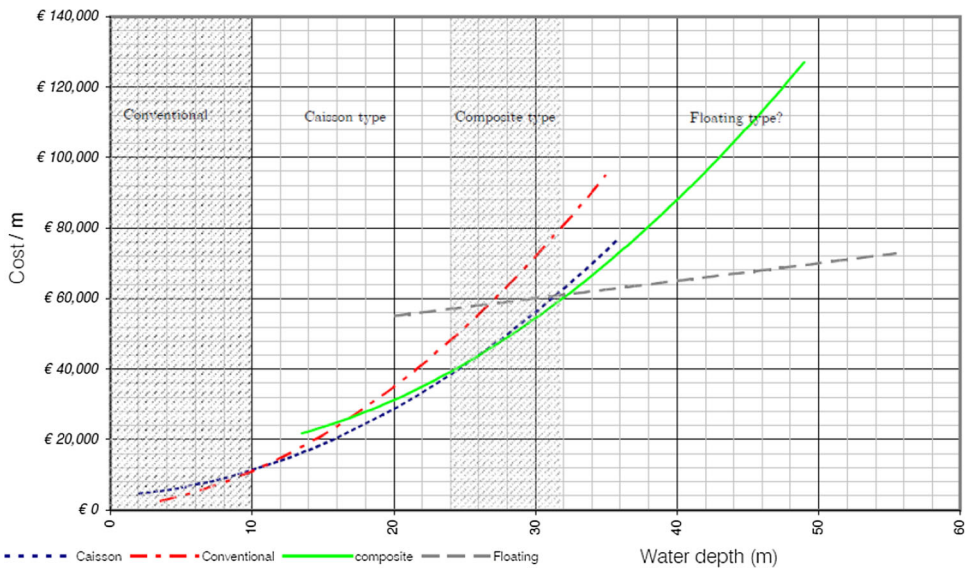

Fig. 2 Costs of different breakwater structures. **a** Mound types, **b** monolithic types, **c** composite types, and **d** floating breakwaters. *Source* Fousert [4]

their design objectives, transmitting larger waves than the ones tolerated by moored ships located at sheltered areas. Moreover, several uncertainties on the magnitude and types of applied loadings on the system, and lack of maintenance cost information lead to conservative design practices which naturally increase the initial project cost. According to Hales [5], a major disadvantage is that floating breakwaters move in response to wave action and thus are more susceptible to structural fatigue problems.

Summarizing, the advantages and disadvantages of floating breakwaters in comparison with conventional protection structures are listed next:

Advantages

- At larger water depths they are more attractive to be applied from an economical point of view;
- Floating breakwaters are transportable. On the other hand, it is worth mentioning that their performance is

very dependent on the local environmental conditions considered at the design stage;
- Applicable at poor soil conditions;
- Very low interference with sediment transport process and water circulation;
- Multiple functions, such as: mooring facilitation, walkway, or parking facility (Monaco floating breakwater).

Disadvantages

- Provide less protection for waves;
- Very sensitive for wave frequencies close to its natural frequency (resonance);
- Less effective for longer waves;
- Dynamic response to the incoming waves can result in fatigue problems and considerable mooring forces;
- Maintenance costs tend to be higher due to the dynamic response.

Most of the floating breakwaters that have already been constructed are restricted to applications involving short period sea states limited to 4 s of peak period (T_p) and 1.4 meters of significant height (H_s). The same panorama was found by Fousert [4], which also concluded that most of the floating breakwaters in operation were designed to protect only small marinas from short crested waves, but their appliance for large-scale floating breakwaters are not yet common.

One of the few examples designed to protect a large harbor is the pier extension of Port Hercules in Monaco. Installed in 2002, the pier is located in a region of approximately 55 m of water depth and composed by a caisson of 352 m long, with a main body 28 m wide, a total depth of 19 m, and a draft of 16 m. An illustrative picture of the cross section of the Port Hercules floating breakwater is presented in Fig. 3. The structure is multifunctional and, as a permanent structure, it has to withstand design storm conditions during its expected lifetime of 100 years.

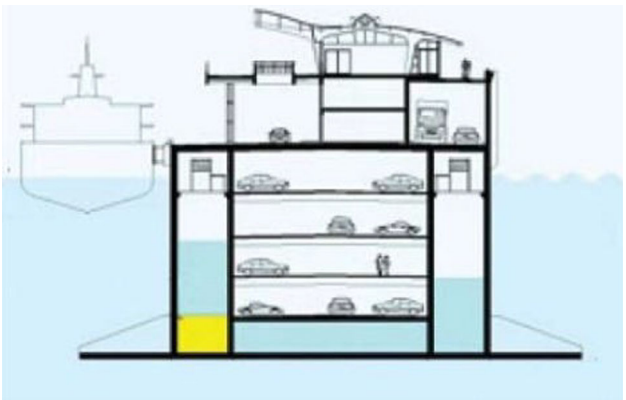

Fig. 3 Cross section of Port Hercules floating breakwater (FDN Engineering)

The floating breakwater of Monaco was designed for 2.8 m of significant wave height and 7.2 s of peak period (FDN Engineering). In these conditions, the floating system is expected to damp 80% of the incident wave energy. On the other hand, for severe conditions ($H_s = 4.9$ m and $T_p = 12$ s) the performance of the breakwater on damping the waves tends to decrease to only 50%, emphasizing the limitations of this type of protection structure on dealing with long waves.

Hales [5] provided a comprehensive survey of floating breakwater types, classifying the different configurations into logical basic groups based on their fundamental features. A more generic classification is given by PIANC [10], which differentiates the floating breakwaters into two groups for design purposes:

- Reflective structures, whose main effect is to reflect the incident wave so that only a small amount of energy may pass beyond them. Examples: Single Pontoon, Double Pontoons, Box, A-frame etc.
- Dissipative structures, where a certain amount of the incident energy is destroyed by friction, turbulence etc. Examples: Scrap tire, tethered float, flexible membranes etc.

These two types of concepts are illustrated in Fig. 4, where H_I, H_R, and H_T are the incident, the reflected, and the transmitted wave heights, respectively.

Once the incident wave interacts with the protection structure, part of the wave is transmitted, reflected, and dissipated. The primary action of the floating breakwater is the inhibition of the vertical component of the wave orbital motion. Other secondary actions include dissipation by eddy generation and friction, as well as some degree of energy reflection. The main parameter to estimate the level of protection is the wave transmission coefficient C_t, defined by Eq. (1). In practice, the lower the transmission coefficient, the better is the concept performance.

$$C_t = \frac{H_t}{H_I} \tag{1}$$

The application of optimization methods in engineering has become very important in the last years due to the requirements concerning cost reduction/efficiency improvement. The application of several numerical methods for the analysis of floating structures has become possible with the increasing of computational power on the last decades, as well as the new interfaces to allow the coupling between software products, including the input/output process. This methodology allows the analysis of several design aspects and the exploration of different

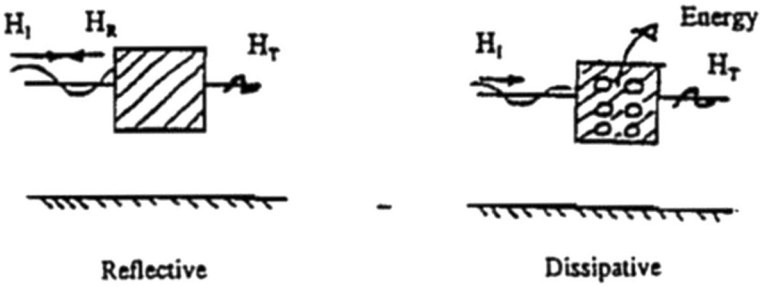

Fig. 4 Reflective and dissipative concepts [10]

geometries (non-traditional), providing a better insight about the key factors in the design and also the expected performance.

The floating breakwater has not been extensively investigated in the literature, especially the ones designed to protect large vessels from sea waves. In this sense, the development of a design methodology incorporating a parametric model coupled to an optimization algorithm may be understood as an interesting approach to assess the most important aspects of the design of a floating breakwater. This paper is focused on the development of a parametric model to evaluate the attenuation capability, stability, structural loads, mooring, and construction costs regarding a floating breakwater for wave attenuation in an LNG terminal, which should be constructed far from the shoreline due to environmental constraints and risks related to this type of cargo. Further analysis regarding the coupling of the parametric model to an optimization algorithm aiming at defining a solution for a specific location will be presented in Part II.

2 Floating breakwater concept

The design vessel considered in the analysis is a large Q-flex LNG carrier with the characteristics shown in Table 1. The critical stage of this operation is to guarantee the safety of the moored vessel, since the mooring equipments (cable, fenders, winches etc.) on the vessel and the on pier itself are designed for static or small dynamic loadings (berthing criteria for fenders) and, therefore, high loads induced by wave motions must be avoided.

Table 1 LNG vessel characteristics

Dimension	Value	Units
Length overall (LOA)	315	m
Length between perpendiculars (Lpp)	303	m
Beam	50	m
Depth	27	m
Draft	12	m
Displacement	146,950	ton

A detailed analysis regarding the mooring integrity assessment using a time-domain dynamic simulation modeling the terminal, cables, fender, and the pier is beyond the scope of this initial design stage and thus a simplified criterion based on ROM [11] was applied, which takes into account only the wave elevation inside the sheltered region. In this criterion, the maximum significant wave height allowed at the vessels' position is 1.5 m, this value being defined as a safety value for the operation of the loading arms involving vessels with 60,000 m^3 of cargo capacity.

The basic layout considered in the analysis can be seen in Fig. 5, where it a minimum circular turning basin area of 315 m radius (PIANC [9] recommendation for conceptual design stage) inside the sheltered region for tug operations is assumed, which also incorporates a safe distance

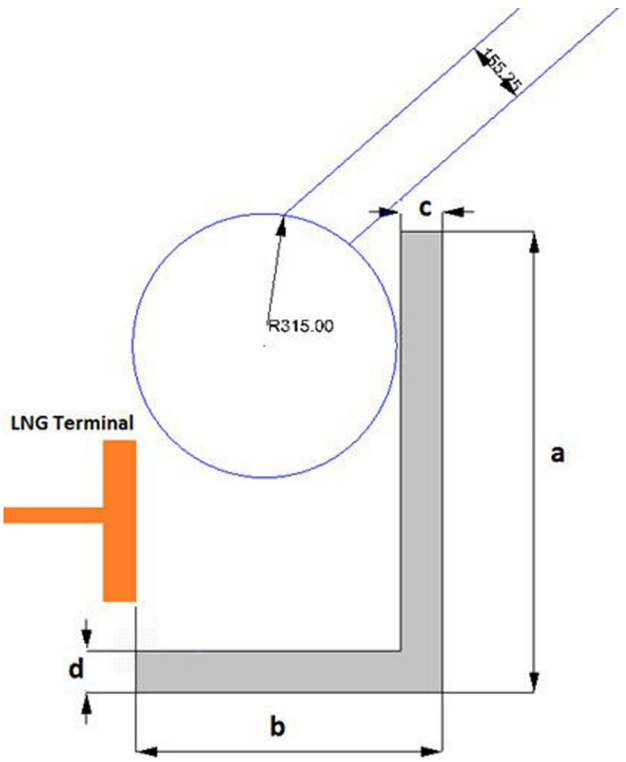

Fig. 5 Basic layout assumed in the analysis

between the terminal and the floating breakwater. The design variables regarding the breakwater structure are the dimensions a, b, c, d, T (draft), and D (depth).

3 Wave attenuation capability

The free surface elevation is computed using the frequency domain first-order potential flow solver WAMIT [15], which is a well-known software applied in the offshore industry for the seakeeping analysis of floating units. Although the application of frequency domain potential flow solvers is not common in the traditional design procedure of fixed breakwaters, in which other methods such as those based on Business equations are more common, the potential flow method was chosen since it can also deal with floating body in waves, especially for long period ones, where the body motions can induce high radiated waves inside the sheltered region, see for instance Koutandos et al. [6].

The results are computed in frequency domain for several regular waves obtaining the free surface elevation response operator defined in Eq. (2), where $A_p(\omega,\alpha)$ is the free surface elevation at a spatial point p of the sheltered region and A_0 is the wave amplitude of the incident wave field outside the breakwater for a wave frequency ω and incident direction α.

$$\mathrm{RAO_P}(\omega,\alpha) = \frac{A_p(\omega,\alpha)}{A_0} \tag{2}$$

The significant wave height at a point p located in the sheltered region is computed using Eq. (3) where $S_\zeta(Hs_0, T_p, \omega)$ is a generic wave spectrum with peak period (T_p) and significant wave height (Hs_0) measured outside and far from the breakwater.

$$Hs_p(T_p, Hs_0, \alpha) = 4\left[\int_0^\infty |\mathrm{RAO_P}(\omega,\alpha)|^2 S_\zeta(Hs_0, T_p, \omega)\mathrm{d}\omega\right]^{1/2} \tag{3}$$

The significant wave height inside the sheltered region is not uniform and changes spatially even for the small area occupied by the design vessel. Therefore, the free surface elevation was computed at 300 points spread in a rectangular shape grid with the vessel dimensions (30 points in the longitudinal direction by 10 points in the transversal one). In such approach, the significant wave height in the sheltered area is calculated taking the mean value, as shown in Eq. (4).

$$Hs_{\mathrm{shelt}}(T_p, Hs_0, \alpha) = \frac{1}{N}\sum_{p=1}^{N_P} Hs_p(T_p, Hs_0, \alpha) \tag{4}$$

In order to validate the proposed methodology, a single fixed breakwater was modeled and the results compared to experimental data from Koutandos et al. [6]. The experimental campaign was performed in a 5 m depth wave flume with, considering a box-shaped model with 2 m width, 1.5 m height, and 2.8 m length.

The results concerning wave propagation are presented in terms of transmission coefficients measured downstream of the model at half wave length (λ), as defined in Eq. (1).

As the experimental test described in Koutandos et al. [6] was conducted in a wave flume assuming the wave flow as two-dimensional, the computational calculations carried out with the three-dimensional code WAMIT had to be accordingly adapted to reproduce the test data. To reduce three-dimensional effects, the breakwater length was increased to 350.0 m based on a sensitivity analysis. The comparison between the numerical predictions and the experimental test is presented in Fig. 6 for 3 breakwater drafts (0.4, 0.5, and 0.67 m), considering distinct values of the ratio of the breakwater beam per wave length.

In general, a good agreement between WAMIT and experimental data for all draft conditions can be noticed, reproducing very well the curve trends, in which the transmission coefficient is increased when the waves become longer. In fact, this was indeed expected, since the breakwater works as a wall for short waves, whereas long waves pass below the model more easily. A better visualization of these effects may be observed in Fig. 7, which presents the wave field pattern upstream and downstream of the floating breakwater for different wave periods.

As may also be observed, one should realize that although the trends were well captured, the numerical model does not provide accurate results for the three longest waves tested in the wave flume, overpredicting the transmission coefficients for all drafts considered. A possible explanation for these deviations refers to the fact that WAMIT does not account for any energy dissipation on the wave field, which certainly occurs in the experiment due to flow separation and vortex shedding at the breakwater bottom edge. On the other hand, it is important to

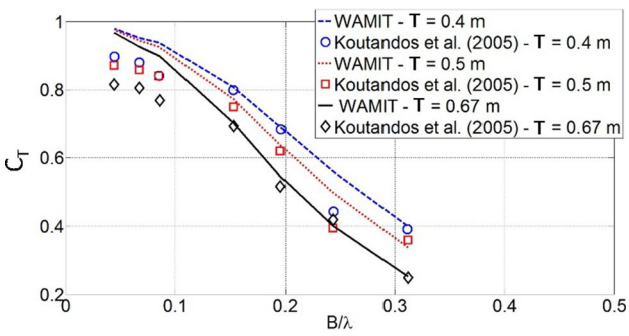

Fig. 6 Comparison between numerical and experimental results of transmission coefficients for different B/λ values and a breakwater with drafts 0.4, 0.5, and 0.67 m

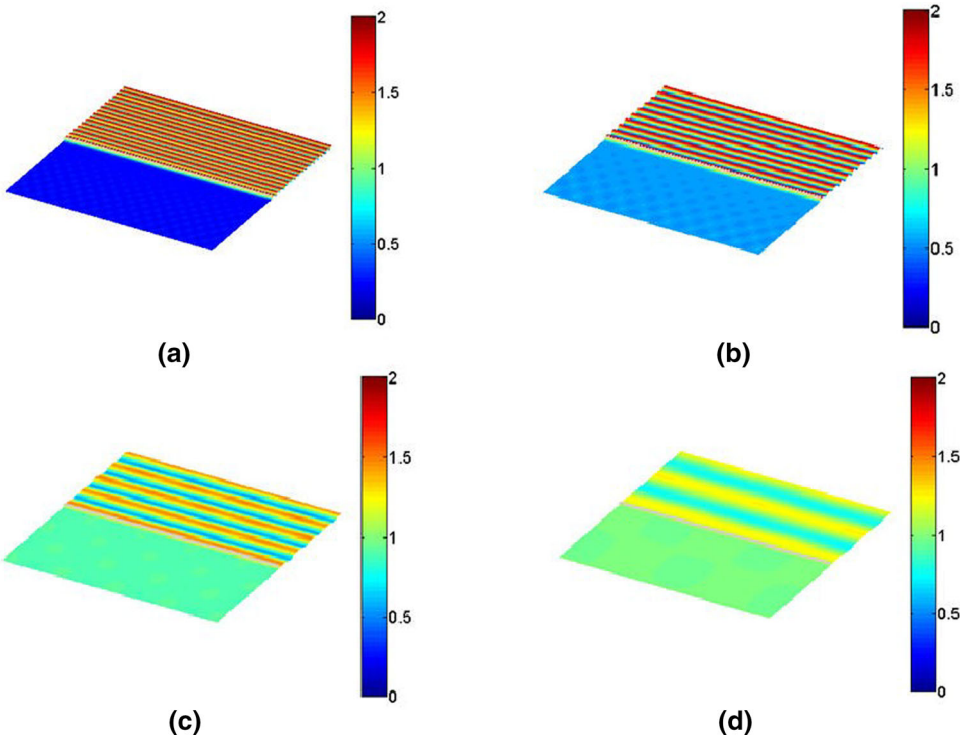

Fig. 7 Wave pattern for different wave frequencies from short to long waves. Incident wave amplitude $A = 1$ m. Breakwater with draft 0.67 m. **a** $B/\lambda = 0.315$; period = 2.02 s, **b** $B/\lambda = 0.195$; period = 2.56 s, **c** $B/\lambda = 0.090$; period = 3.77 s, **d** $B/\lambda = 0.040$; period = 5.66 s

emphasize that by disregarding any dissipation on the wave flow, WAMIT provides more conservative results in terms of wave elevation, being a very useful tool especially at the conceptual stage of the floating breakwater design.

In the free floating simulations, the moments of inertia and position of the center of gravity are very important to define the body dynamics properly and since there is a lack of available data in the literature, a structural model was developed, as presented next, which is also used for the cost estimation.

3.1 Structures and cost estimation

The design of floating breakwaters should take into account the strength and serviceability [10], since the design must ensure an adequate margin of safety to prevent failure during its lifespan. According to PIANC [10], large floating breakwaters are built by joining blocks (or caissons) of reinforced concrete, as shown in Fig. 8.

This strategy of using several concrete blocks has already been applied in several ports (i.e.,: Açu Superport in Brazil) and offshore industry (see examples in Fig. 9).

At this stage of the design, the main challenge is to define the structural dimensions of the concrete blocks to support the external loads. According to PIANC [10], the following loads should be considered in the design:

- Wave-induced force (EW)
- Current drag forces (EC)
- Wind drag forces (EW)
- Dead loads (DL)—total weight of concrete structure (caissons), connections, and mooring
- Live loads (LL)
- Deformation loads caused by temperature effects, prestress, shrinkage, and creep (TL)
- Dynamic loads due to breakwater motions.

The loads shall be combined with safety factors depending on the probability of occurrence. All loads should be considered with a recurrence period of 50 years, but the first one (EW). The current design requires the floating breakwater strength to support the loads defined in Eq. (5).

$$U = 1.2(\mathrm{DL} + \mathrm{TL}) + 1.2\mathrm{LL} + 1.3(\mathrm{EW} + \mathrm{ED} + \mathrm{EC}) \quad (5)$$

The material selected for the floating breakwater structure is the reinforced concrete with longitudinal and transversal bars. The walls were considered as solid slabs of rectangular shape clamped into the four edges. The slabs were designed to resist local structural loads, defining the minimum length, width, and thickness.

The material considered in the analysis was the C50 class concrete with the specific characteristics for harsh environmental conditions [10], assuming a safety factor of 1.4 and the maximum traction and shear stress limits of 4.2 and 1.05 MPa, respectively, according to DNV [3] standard. The steel assumed in the analysis has 500 MPa yield strength and an additional 50 mm thickness outer cover is applied to prevent corrosion and erosion. The ratio of steel

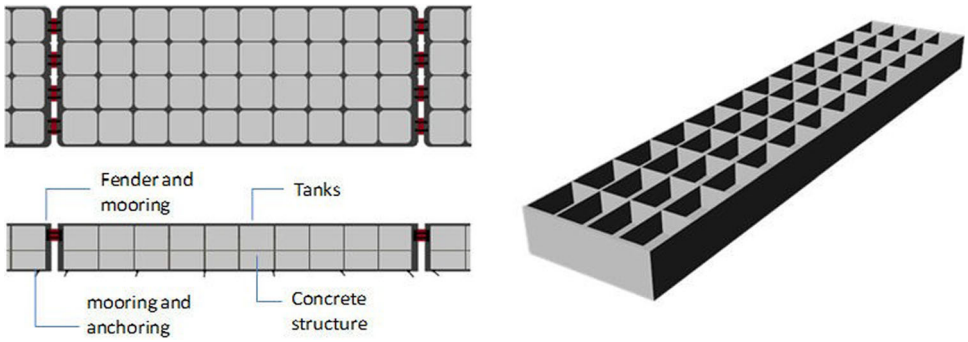

Fig. 8 Example of caisson block for breakwater construction (*right*) and the elements (fender and mooring) for the connection of the blocks

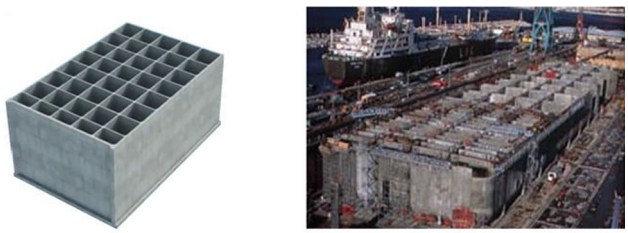

Fig. 9 **a** Caisson type of Açu Superport and **b** NKOSSA BARGE [14]

to concrete is between 1.0 and 1.5%, providing an additional 4.0–6.5 MPa of maximum traction stress capability.

Since the floating breakwater has large dimensions, the hydroelastic effects can also be important, see for instance Andrianov [1], Suzuki [13], and Miyajima et al. [8]. However, in this initial design stage, these effects were neglected, assuming a multi-rigid structure. The loads assumed in the computations are the hydrostatics, current, mooring tensions, and waves, the latter assumed as an undisturbed wave field.

The loads and deformations in reinforced slabs in two directions are calculated assuming the theory of plates based on Hooke's Law for a homogeneous and isotropic material, given by Eq. (6), where w is the vertical displacement, p is the load, and D the bending stiffness, as given by Eq. (7).

$$\frac{\partial^4 w}{\partial x^4} + 2\frac{\partial^4 w}{\partial x^2 \partial y^2} + \frac{\partial^4 w}{\partial y^4} = \frac{p}{D} \tag{6}$$

$$D = \frac{Eh^3}{12(1-v)^2} \tag{7}$$

The solution of Eq. (6) is rather complex and, therefore, it is assumed a simplified solution with the maximum bending moments computed by Eq. (8), where μ is a coefficient defined according to the slab length per width ratio and l_x is the smallest void of the slab.

$$M = \mu \frac{p l_x^2}{100} \tag{8}$$

The thickness of the slab is defined based on Eq. (9) assuming a width of 1.0 m, where k_c is a coefficient that changes with the type of concrete.

$$h = \sqrt{\frac{k_c M}{100}} + 50 \tag{9}$$

The minimum sectional armor area is computed from Eq. (10), where k_s is a coefficient dependent on both steel type and ratio between the position of neutral axis and the thickness of the slab section.

$$A_S = \frac{k_s M}{h - 50} \tag{10}$$

The hydrostatic loads are computed between the balance of weight and buoyancy ($\rho_W gz$), while the hydrodynamic loads due to wave are computed assuming the undisturbed pressure field in shallow water under the potential flow hypothesis, given by Eq. (11), where A is the wave amplitude, k the wave number, θ_W is the wave direction, and h the water depth.

$$P_d = \rho_W g A \left[\frac{\cosh(k(z+h))}{\cosh(kh)}\right] \cos(\theta_W) \tag{11}$$

The current drag is computed using Eq. (12), where $C_S(\theta_c)$ is the current coefficient (taken from a box structure), A is the projected area, and V the current velocity.

$$F_c = \frac{1}{2}\rho_W C_S(\theta_c) A V^2 \tag{12}$$

The mooring loads are computed by Hooke's law ($F_M = K\Delta x$), where K is the mooring stiffness and Δx the body offset.

The current velocity assumed in the analysis was 1.5 knots following [10] recommendations for a pier and a maximum significant wave height of 6.5 m in a range of periods between 7 and 16 s for all wave directions. The breakwater is modeled following the multi-rigid approach proposed by Saleh [12] for mega floating concrete bridges, since the structure is elastic and there is absorption and dissipation of energy among the parts, reducing the stresses compared to "fully" rigid body structure. Saleh [12]

studied the structural stresses under waves shorter, equal, and longer than the concrete block length, concluding that the most critical condition was for waves with the length of the block, which is called the critical wave length.

The analysis is performed considering the concrete block in the middle of the structure with the critical wave length, where the moment reaches the maximum value in the middle section and is null in the ends. On the other hand, the maximum shear forces are achieved in 25 and 75% of the block length, also with null values in the ends. These loading conditions are illustrated in Fig. 10, where the blue box is a concrete block located in the middle of the structure.

The definition of the critical wave is also dependent on the wave height distribution according to the specific wave conditions in the installation site. For the selected location, the critical wave calculated is 6.5 m of significant wave height and 12.5 s of peak period.

The shear forces in each section of the block are calculated by Eqs. (13) and (14), assuming $Q(0) = Q(L) = 0$ and $M(0) = M(L) = 0$.

$$Q(x) = \int_0^x p(y)\mathrm{d}y, \quad 0 \leqslant x \leqslant L \tag{13}$$

$$M(x) = \int_0^x p(y)y\mathrm{d}y, \quad 0 \leqslant x \leqslant L \tag{14}$$

The loads are combined in *XY* plane considering the mooring forces projected in the horizontal plane combined to the current loads and wave pressure, obtaining the loading curves shown in Fig. 11a. The loads, shear forces, and bending moment considered in the *XZ* plane can be seen in Fig. 11b.

The torsion moment acting on the structure is also computed in the plane *YZ*, providing the results shown in Fig. 12, considering only the hydrostatic and wave loads.

Following the methodology described earlier, the minimum ratio between breadth and draft is defined to guarantee the block buoyancy, assuming also an additional 20% design margin to take into account the mooring weight, connection materials, and uncertainties related to the construction process. The draft is assumed as 75% of the depth considering ballast sand to achieve neutral floatation.

The ratio of lightweight per displacement by the ratio of draft per breakwater sectional width (*T*/*c* or *T*/*d*) can be seen in Fig. 13, where it can be verified that a minimum 0.2 *T*/*c* (or *T*/*d*) is required to guarantee the concrete block buoyancy in the design draft. If a smaller ratio is assumed, the draft will increase, reducing the available freeboard, which may be undesirable in order to avoid wave overtopping. In these cases, the floating breakwater design is assumed as unfeasible. On the other hand, if a higher *T*/*c* (or *T*/*d*) is selected, additional sand ballast must be added to achieve the design draft, which is important to guarantee the breakwater attenuation capability.

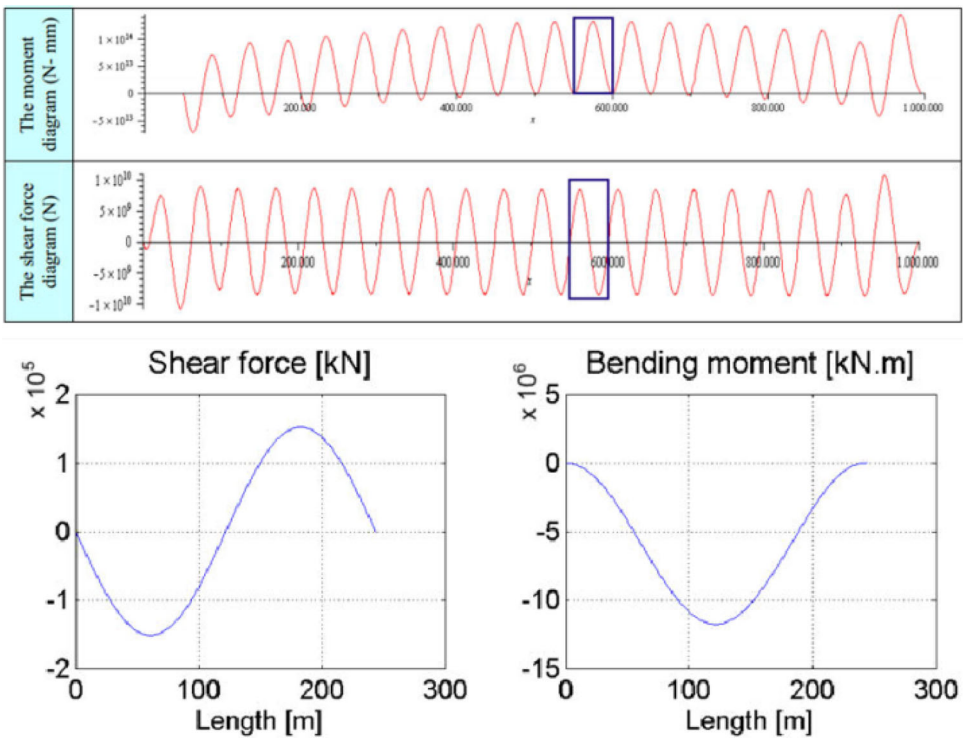

Fig. 10 Shear force and moment applied in a block located in the middle of the floating breakwater (adapted from Saleh [12]) and the shear forces and bending moments considered in the analysis (the signal is different due to the wave phase considered)

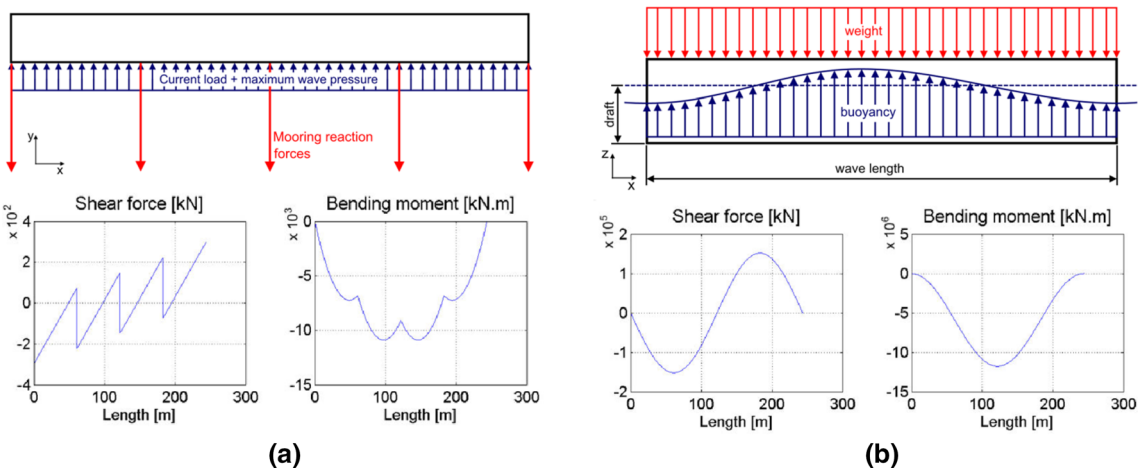

Fig. 11 Loads considered in the *XY* and *XZ* planes

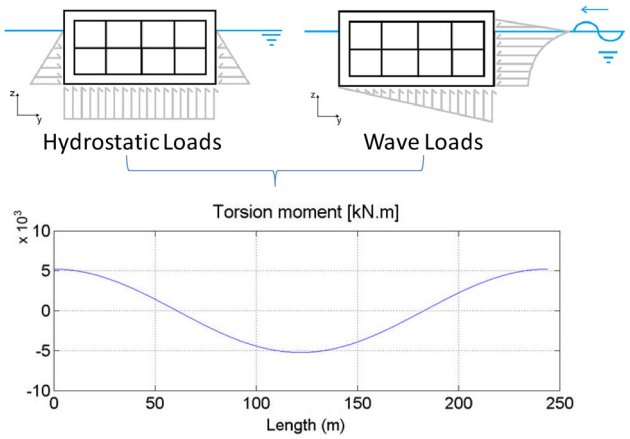

Fig. 12 Loads considered in the *YZ* plane in the structural assessment

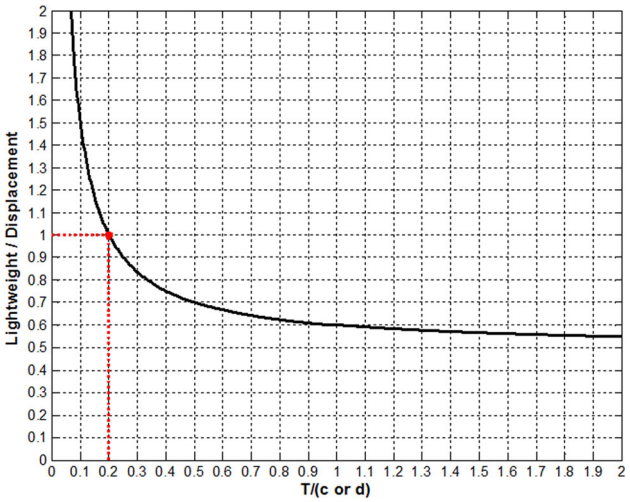

Fig. 13 Ratio of lightweight per displacement by draft per width

The vertical center of gravity position is defined based on Eq. (15), where m_i and VCG_i are the ith element mass and vertical center of gravity position. The sand ballast density is assumed as 2500 kg/m^3. The caissons have several internal walls (compartments) that are equally distributed along the length and breadth of the block. The moments of inertia are computed analogously.

$$\mathrm{VCG} = \frac{\sum m_i \mathrm{VCG}_i}{\sum m_i} \tag{15}$$

The cost estimation of each block is performed assuming the concrete cost as 743.5 US$/m^3, already taken into account material, labor, shipyard, and indirect costs, defined based on a market survey. The results regarding the construction cost per breakwater unit length for several draft and breadths are summarized in Fig. 14, where the

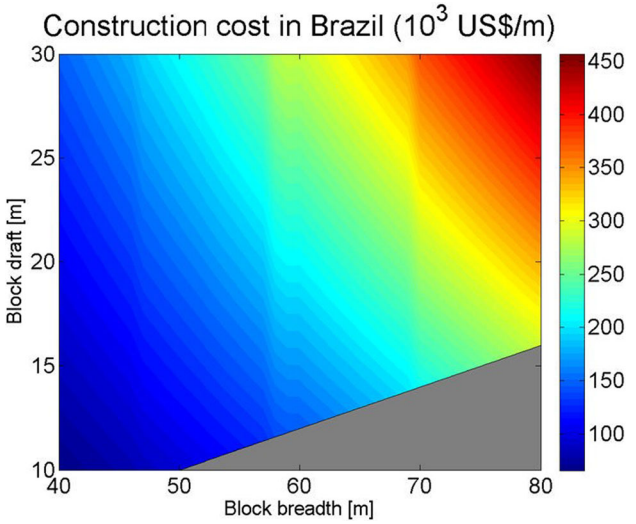

Fig. 14 Estimated block construction cost per length for different drafts and breadths

gray area are unfeasible solutions due to the ratio of T/c, as discussed previously.

Due to the lack of available data, it is quite difficult to verify the accuracy and validation of the proposed methodology. Therefore, only two validation exercises were conducted. The results are based on data from the N'Kossa platform, a floating production unit operating offshore in the Republic of Congo (200 × 46 × 16 m—concrete volume 26.000 m^3) and the caisson blocks of Açu Superport (67 × 25 × 34 m) in the Brazilian coast. The comparison can be seen in Table 2 including the estimate based on Fousert [4] curves.

A simplified result concerning cost estimate per Floating Breakwater displacement can be seen in Fig. 15, considering several feasible dimensions, where a linear trend regarding the increase of structural cost with the breakwater displacement can be verified. A linear fit equation is defined based on Eq. (16) and the upper limit considering 99.9% of coverage is defined by Eq. (17).

$$\bar{C} = 1.3256 \times 10^{-5}\Delta - 2.99 \text{ (MUS\$)} \quad (16)$$

$$C_{99.9\%} = 1.752 \times 10^{-5}\Delta - 2.99 \text{ (MUS\$)} \quad (17)$$

4 Hydrodynamic performance

The hydrodynamic performance of the floating breakwater is investigated concerning four key factors in terms of wave attenuation: wave period, direction, water depth, and the floating unit motions.

In order to verify the protection capability achieved in the numerical computations, the results concerning diffraction maps are presented in the entire field inside and around the floating breakwater. The geometry chosen for this analysis has the geometry characteristics shown in Table 3 and the results are presented in terms of diffraction maps (amplification factor) for a sea state with a unitary significant wave height.

The diffraction maps provide a better insight concerning the physical phenomenon regarding wave attenuation, see for instance Fig. 16 summarizing the simulation conditions.

Table 2 Comparison of cost estimate (US$)

Estimate	N'Kossa	Ac¸u block
Numerical code	23,248,003	3,258,548
Fousert [4]	21,681,416	3,537,823
Construction cost	–	3,097,345

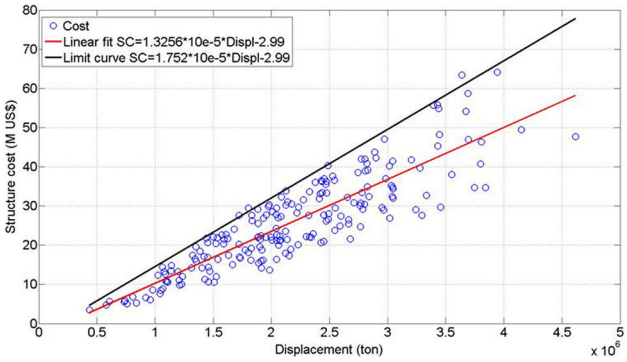

Fig. 15 Construction cost per displacement for several floating breakwater dimensions and linear regression (*red lines*). The linear regression with coverage of 99.9% is the *black line* (Color figure online)

Table 3 Breakwater characteristics

Dimension	Value	Units
a	729	m
b	705	m
c	75.5	m
d	57.1	m
T	16	m
Displacement	1,488,891	ton

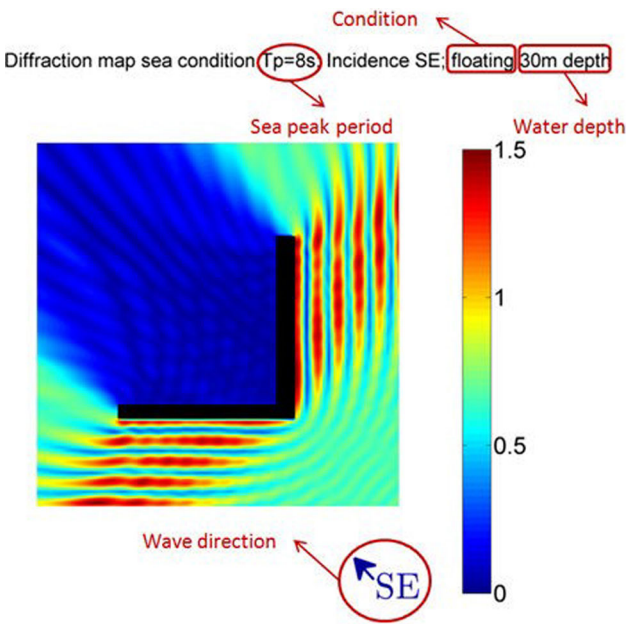

Fig. 16 Example of diffraction map

4.1 Wave period effect

The effect of wave period and direction is important in the diffraction wave pattern induced by the floating

breakwater. In order to verify the influence of the wave peak period, the values of 8, 12, 16, and 20 s were selected in this study ranging from a short local sea state condition until a long swell, both conditions very common in South America basin. The influence of wave direction is evaluated comparing the wave directions S, SE, E, NE, and N, the first four directions assumed as the main ones in terms of breakwater design condition and the last one as a critical one.

The comparisons concerning both wave period and direction in terms of diffraction coefficients can be seen in Figs. 17, 18, 19, 20, and 21. It can be verified that for the shortest waves evaluated (8 and 12 s), the floating structure reflects the wave propagation almost completely, avoiding the transmission of wave energy for almost all the area, but for some points close to the breakwater edges. The attenuation capability reduces with the increasing of the wave period regardless of the wave direction, since the long waves can both contour and flow below the floating structure. It can also be verified a reduction of the sheltered region due to the higher diffraction in the edges, which can also be verified by the reduction in the angles that provide lower wave elevations in relation to wave direction. As expected, the best attenuation capability is achieved in the SE incidence direction, since even the long waves cannot contour the breakwater completely. On the other hand, the S and E directions provide almost the same attenuation level with a significant increase in wave height for long waves, that can be attributed to both waves propagating along the edges and resonant effects induced by the internal walls or body motions. In fact, these effects are also intensified due to the absence of dissipation terms in the potential formulation.

4.2 Influence of water depth (underkeel clearance) and body motions

In order to define the influence of the body motions on the wave elevations, the same structure is also simulated in a higher water depth (70 m), since a large variation of the added mass due to the change of underkeel clearance is expected. The investigation is performed also considering a hypothetical fixed breakwater operating in both 30 and 70 m water depth to provide a better insight of the influence of the body motions and the water that flows below the structure keel. The results can be seen in Figs. 22, 23, and 24 concerning waves with peak period of 8 and 20 s under southward wave incidence.

It can be verified that for short waves there are almost no differences comparing the floating and fixed breakwater

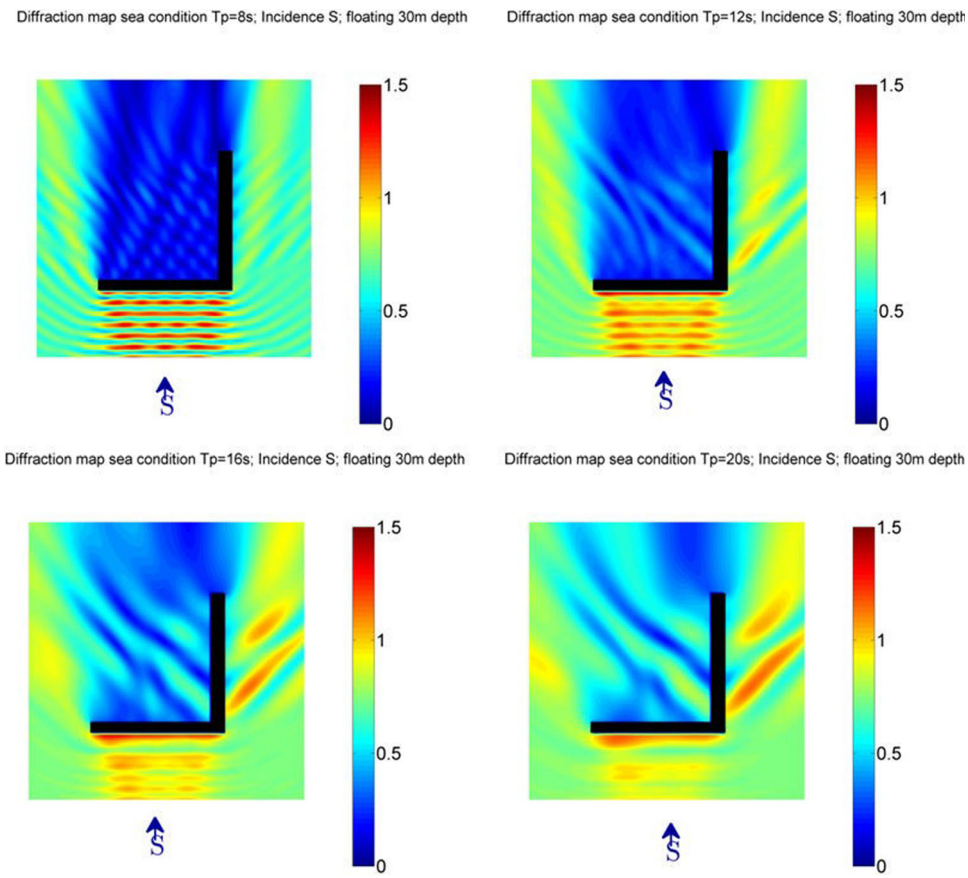

Fig. 17 Breakwater attenuation performance for different peak period 8 (*top left*), 12 (*top right*), 16 (*bottom left*), and 20 s (*bottom right*)—southward wave direction, 30 m water depth

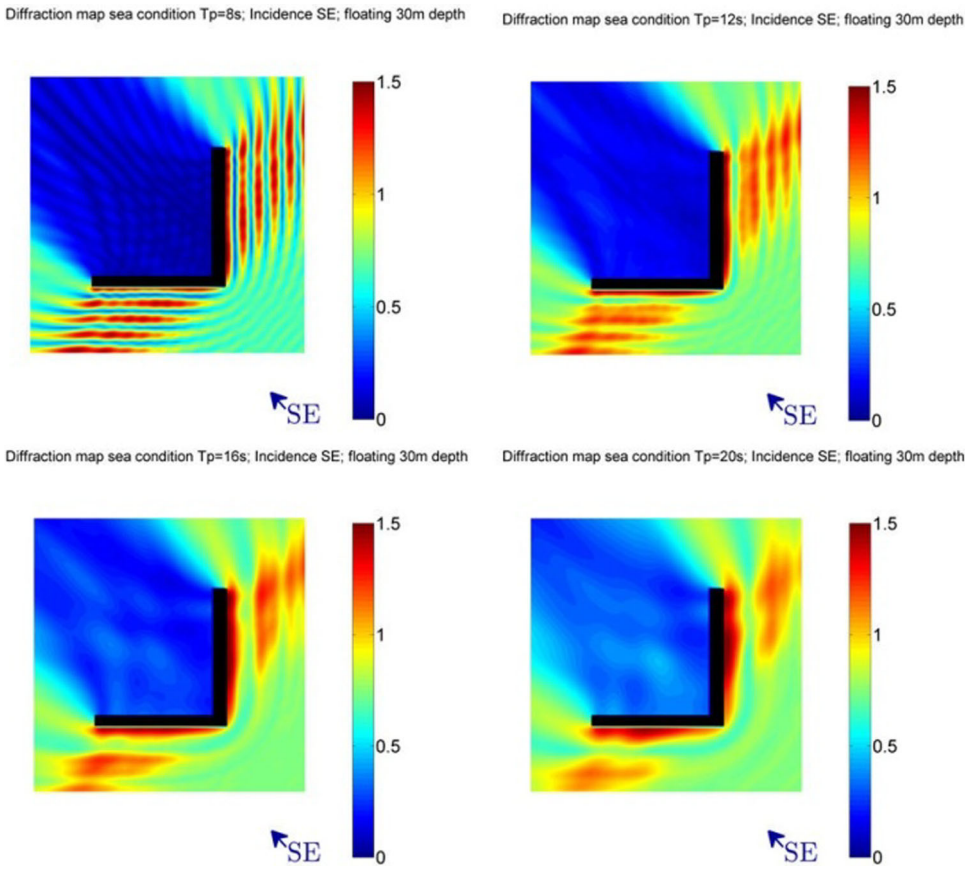

Fig. 18 Breakwater attenuation performance for different peak period 8 (*top left*), 12 (*top right*), 16 (*bottom left*), and 20 s (*bottom right*)—southeast wave direction, 30 m water depth

regardless of the water depth, which can be explained based on the wave body interaction physics. For short waves (~8 s), the breakwater works almost like a wall, with almost no transmitted wave and the structure motions are very small since the natural periods of heave, roll, and pitch are higher. In this condition, there are no radiated waves inside the sheltered region induced by the body motions. Moreover, the short waves cannot "pass" below the keel of the floating breakwater, therefore the free surface elevations in the vessel region are associated only to diffraction effects originated from the breakwater corners, which create a "ring" wave pattern that can contour the structure and reach the sheltered region.

For intermediate waves (12 s), it can be verified that for 30 m of water depth, the performances of the fixed and floating concepts are similar in the vessel region, although there are some points with higher free surface elevations in the internal region of the floating concept than the fixed one. However, for 70 m water depth, the floating concept produces a higher water elevation in the middle of the breakwater compared to the fixed concept. The main reason is because intermediate waves can pass below the floating breakwater keel, reaching the middle region, whereas in the fixed case it is not possible because the breakwater is supported by the bottom. Besides, in this wave range, the floating breakwater presents heave and roll motions that radiate waves inside the breakwater. The bottom can also deform the wave orbital appreciably if waves are long, therefore, there are some differences in the breakwater performance due to water depth.

As a consequence of bottom interaction, the wavelength reduces in shallow water. Therefore, the differences in the fixed breakwater due to water depth are mainly related to differences in wavelength, which also changes the diffraction wave pattern.

For long waves (20 s), the performance of the floating breakwater is not good since the waves can "pass" under the keel and produce high motions in the structure, which generates high wave heights inside the sheltered region. However, most of the wave occurrences close to the coast usually have low period (less than 12 s) and, therefore, the low performance in high period waves should not contribute to the operational downtime appreciably. It is clear that a complete analysis would require the installation site definition to verify the expected uptime. The breakwater motions can be evaluated in terms of the response amplitude operators (RAOs) in 6 degrees of freedom. Heave motions are the most important factors to radiated waves as shown in Fig. 25 (considering southward and northeast wave incidences for a 30 and 70 m water depth).

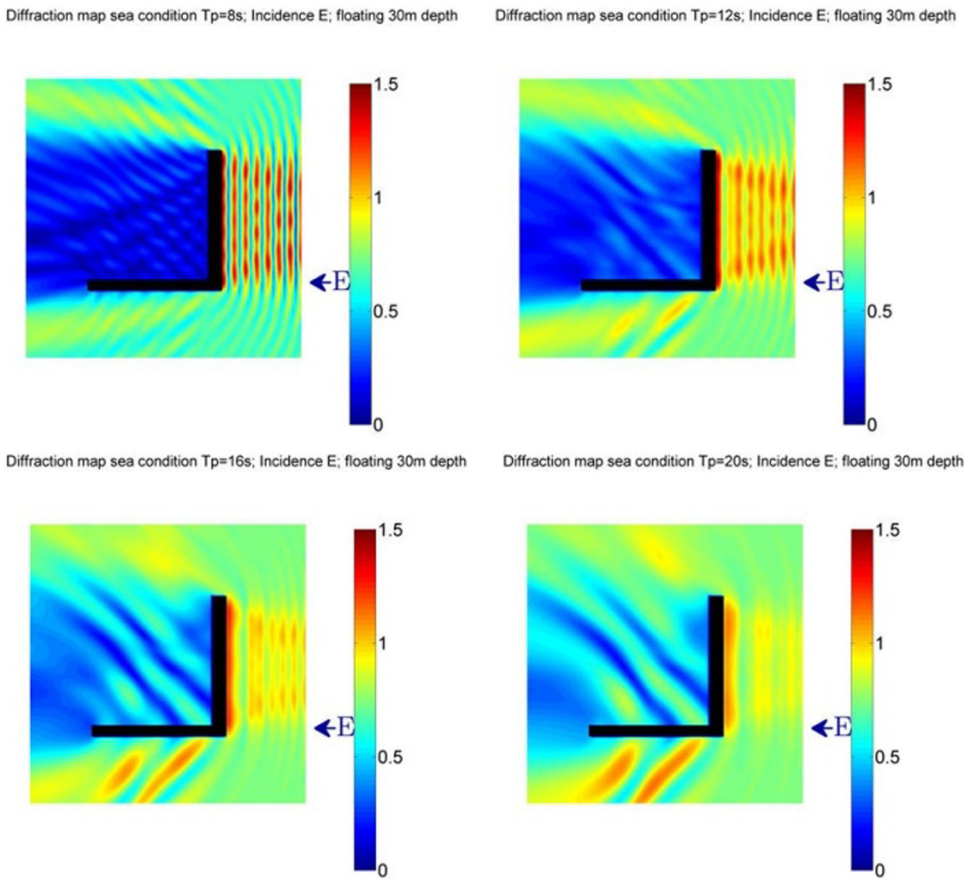

Fig. 19 Breakwater attenuation performance for different peak period 8 (*top left*), 12 (*top right*), 16 (*bottom left*), and 20 s (*bottom right*)—east wave direction, 30 m water depth

For the southward wave incidence there is almost no motion for 8 s wave period. The amplification factor is less than 5%, meaning that for each meter of incident wave, the floating breakwater heaves 5 cm, regardless of the water depth. Therefore, only a small portion of the free surface elevation inside the breakwater is associated to body motions. On the other hand, for 16 s waves, the breakwater moves about 0.5 m for each 1 m of incident wave amplitude, generating a considerable amount of radiated waves. In the case of the northeast wave incidence, the heave RAO is lower mainly for high period waves. It can also explain the differences concerning the attenuation factor presented earlier.

The heave motions are similar in 8 and 16 s considering the 30 and 70 m water depth for south direction. Therefore, the allowable wave height (the maximum significant wave height considering ROM [11] wave elevation criterion) outside the breakwater in these periods are almost the same, as can be verified in Fig. 25. However, for wave period of 12 s, the heave responses are smaller for 30 m water depth compared to the 70 m one. The allowable wave height becomes higher for the 30 m water depth. The main reason for these differences in the motion response is the increase of added mass with the reduction of water depth, which provides an increase of the natural period with the decrease of water depth. A similar trend can also be verified for the East wave incidence.

In the case of Northeast wave incidence, the body motions are smaller for both water depths compared to the south incidence, thus the allowable wave height is similar for both water depths and higher for the Southward wave incidence, confirming the importance of the breakwater motions on the free surface elevation. It should also be noticed that this insight is only a simplified analysis since the complete computation should take into account the entire wave energy spectrum.

The results considering the maximum allowable significant wave height reveal that for the wave directions considered in the design (S, SE, E, and NE), the fixed breakwater works better for long period waves. The body motions and the wave energy that propagates underkeel are important to the wave elevation in the sheltered region. On the other hand, for the other wave directions (N, NW, W, SW) the floating concept works better for long waves. It is also interesting to verify that for short waves coming from E and S directions, the floating concept is better for short waves due to small differences from the edges.

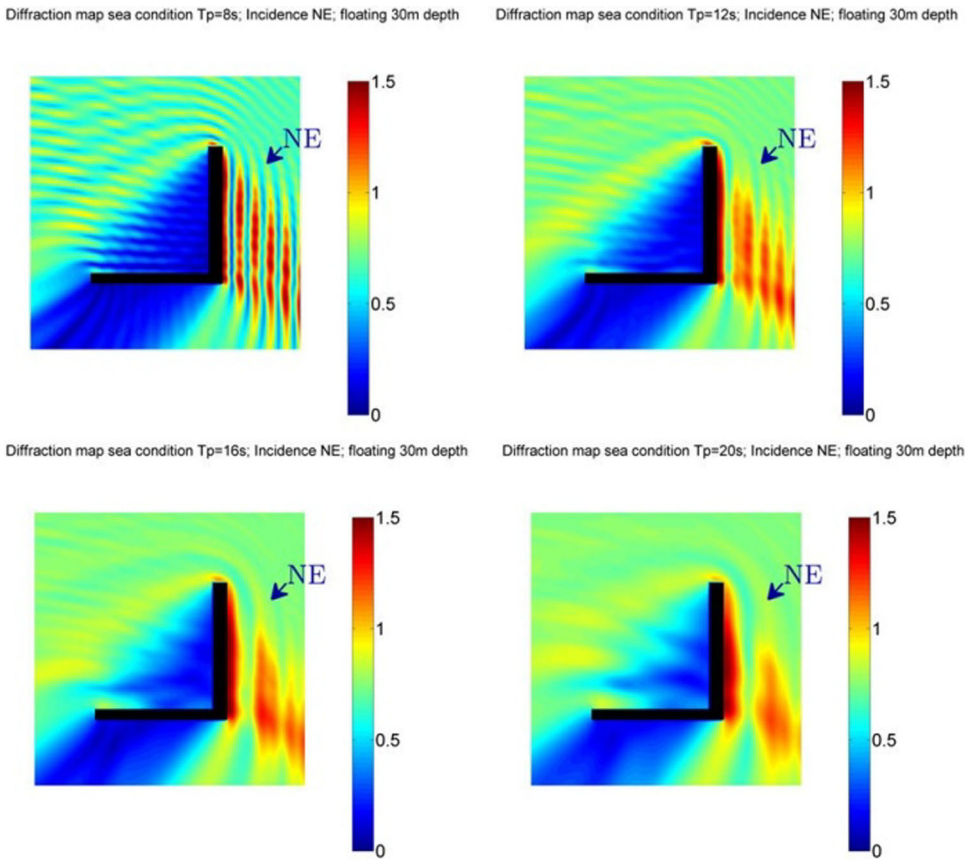

Fig. 20 Breakwater attenuation performance for different peak period 8 (*top left*), 12 (*top right*), 16 (*bottom left*), and 20 s (*bottom right*)—northeast wave direction, 30 m water depth

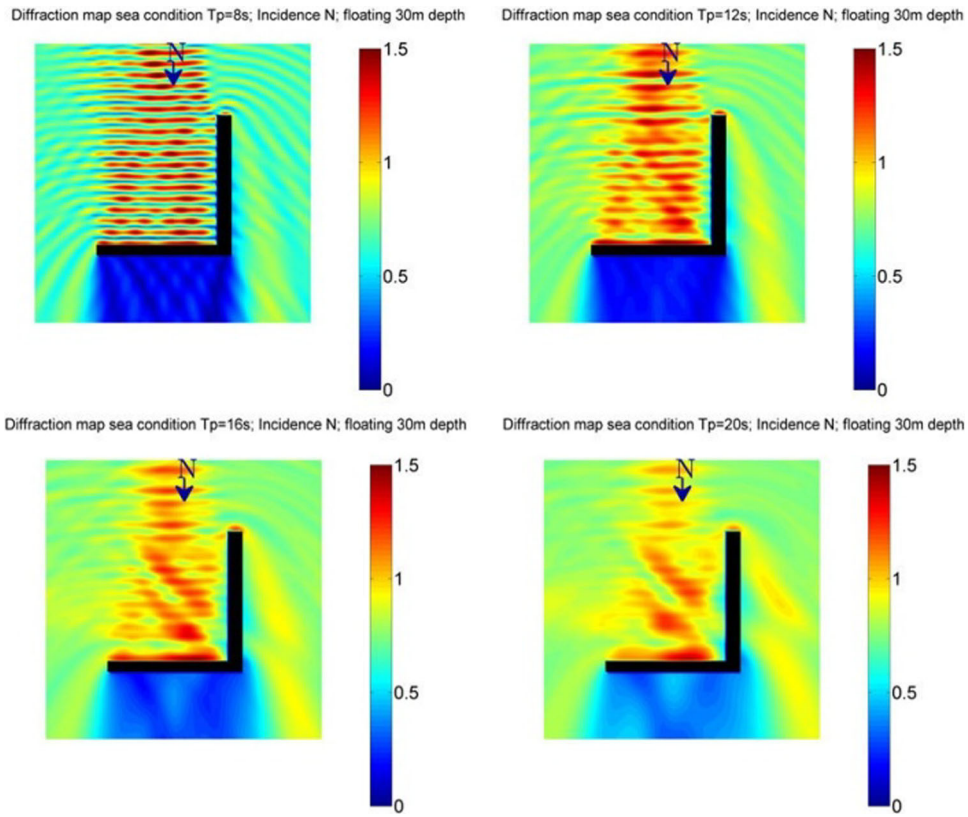

Fig. 21 Breakwater attenuation performance for different peak period 8 (*top left*), 12 (*top right*), 16 (*bottom left*), and 20 s (*bottom right*)—northward wave direction, 30 m water depth

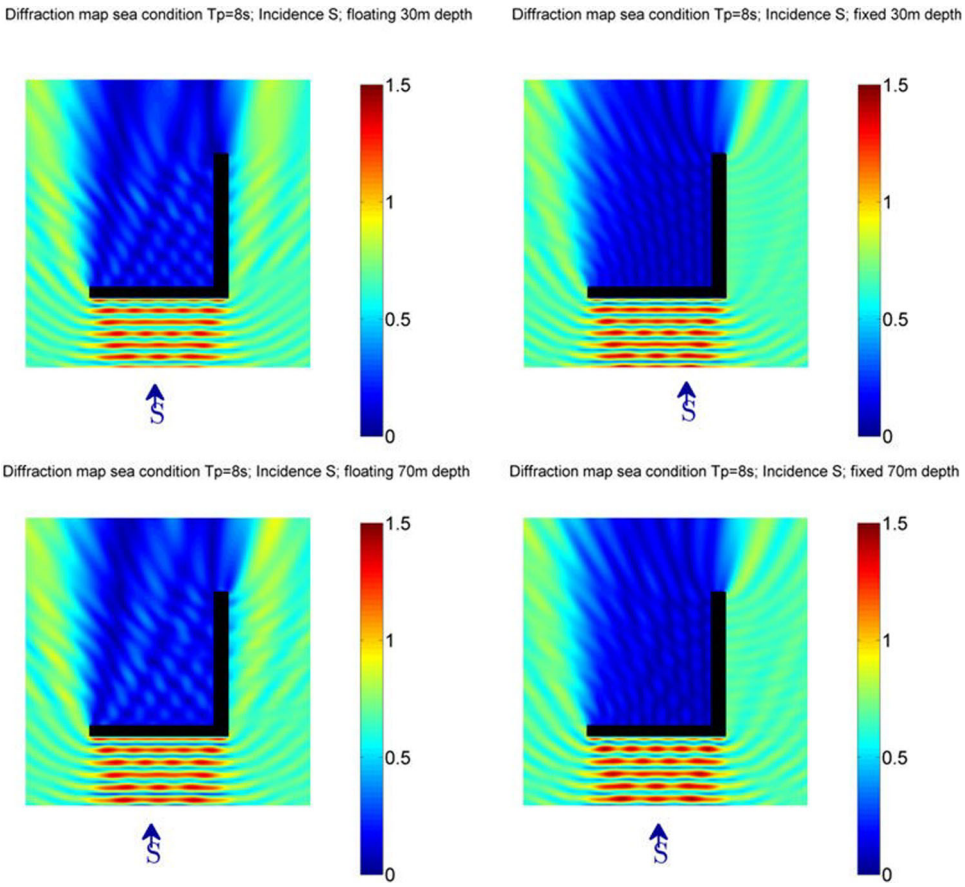

Fig. 22 Breakwater diffraction coefficient for fixed (*left*) and floating (*right*) breakwaters. 30 m water depth (*top*) and 70 m water depth (*bottom*)—8 s peak period

4.3 Influence of mooring arrangement

The results presented earlier verified the great influence of the body motions on the wave elevation, meaning that reducing the heave motion improves attenuation capability. To verify the body motion contribution to the free surface elevation, the same geometry was evaluated without any motion, by representing the floating structure as if it was a tensioned anchored system, similar to a Tension Leg Platform (TLP). In such situations, the heave natural period becomes very small due to the high vertical stiffness of the tendons.

It should be noticed that the first analysis focused only the diffraction capability. Therefore, the mooring system analysis itself was not performed at that stage.

The comparison concerning the floating, TLP, and fixed breakwater can be seen in Fig. 26 for a 16 s sea state and south incidence for both 30 and 70 m water depth. It is remarkable that the motion reduction also decreases the free surface elevation inside the breakwater, mainly in the 30 m water depth, which means that if a tensioned mooring system is feasible to be applied, the improvement in terms of attenuation capability would be clear. The difference concerning the attenuation capability between the fixed and TLP concepts is that in the second condition the long waves can pass "below" the keel and reach the vessel position.

Besides the TLP, there are also other possibilities like a taut leg mooring system, which can increase the vertical stiffness of the system compared to the usual spread mooring using catenary mooring lines. The mooring system analysis would require a detailed study concerning the operational site to verify the soil properties and constraints (for example coral reefs) to define the mooring arrangement feasibility.

5 Breakwater stability

The breakwaters generated by the parametric model have a "L" shape and, therefore, there is no symmetry plane and the axis of minimum metacentric height should be computed during initial stability computation. It should be noticed that the initial stability is a basic criterion for the structure feasibility and no additional criteria were found from the classification society rule. However, the initial metacentric height is a good figure for the stability level of the floating structure.

The initial stability is computed from Eq. (18), where KG is the vertical center of gravity (computed by the

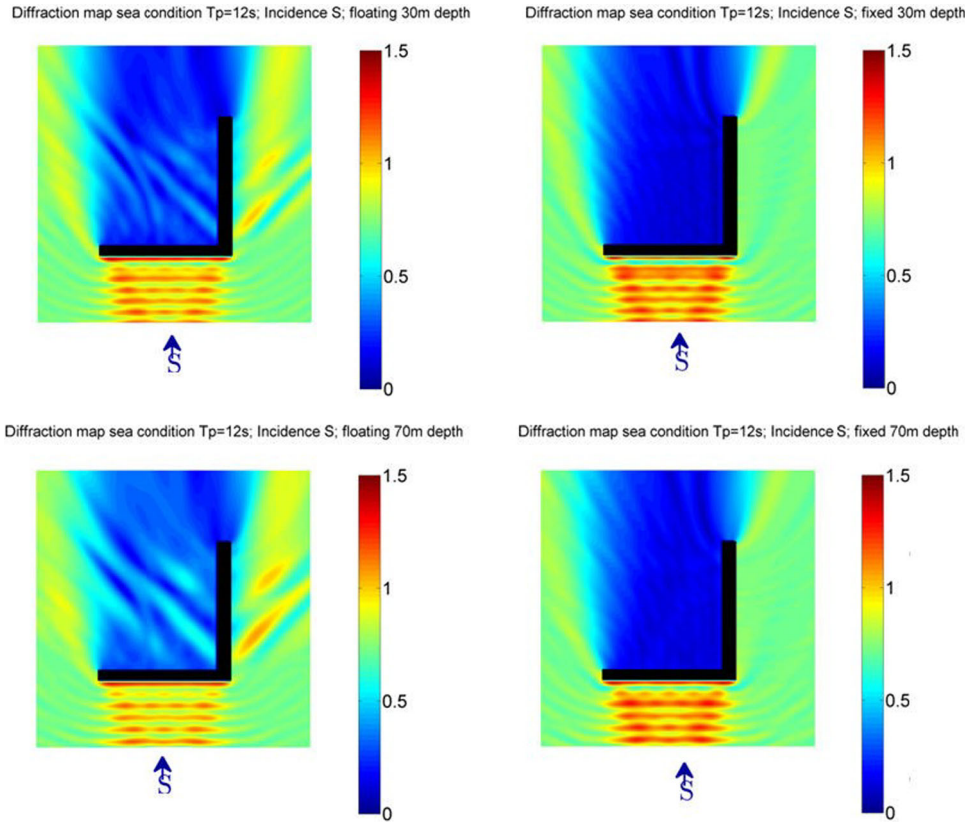

Fig. 23 Breakwater diffraction coefficient for fixed (*left*) and floating (*right*) breakwaters. 30 m water depth (*top*) and 70 m water depth (*bottom*)—12 s peak period

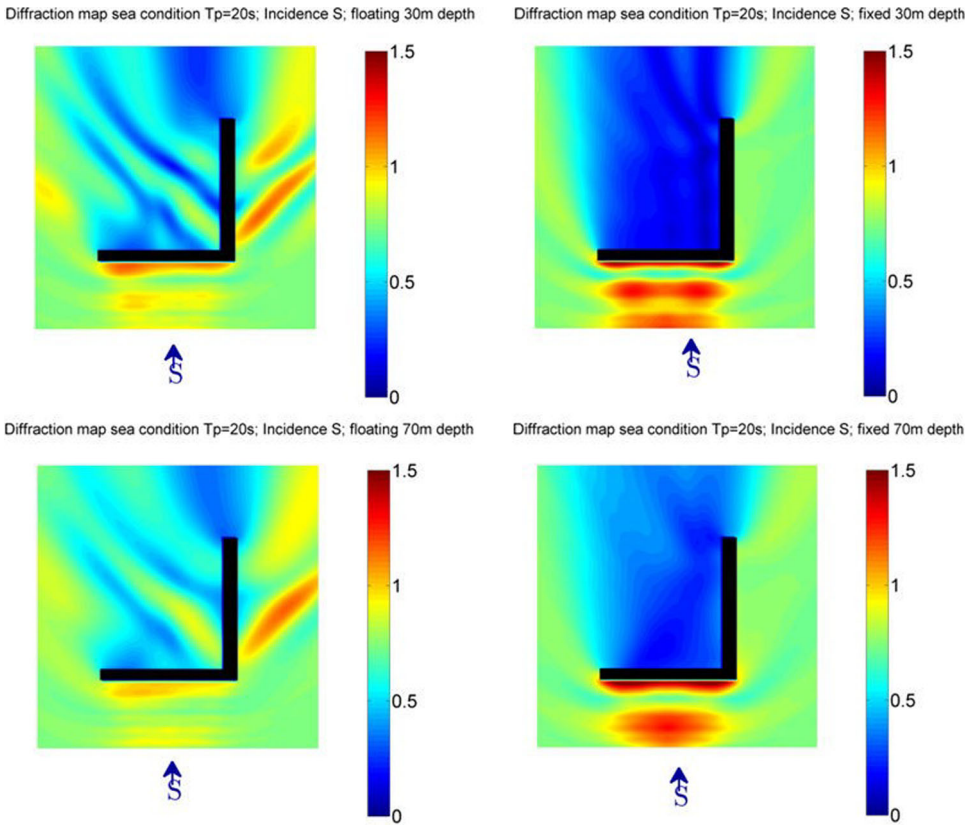

Fig. 24 Breakwater diffraction coefficient for fixed (*left*) and floating (*right*) breakwaters. 30 m water depth (*top*) and 70 m water depth (*bottom*)—20 s peak period

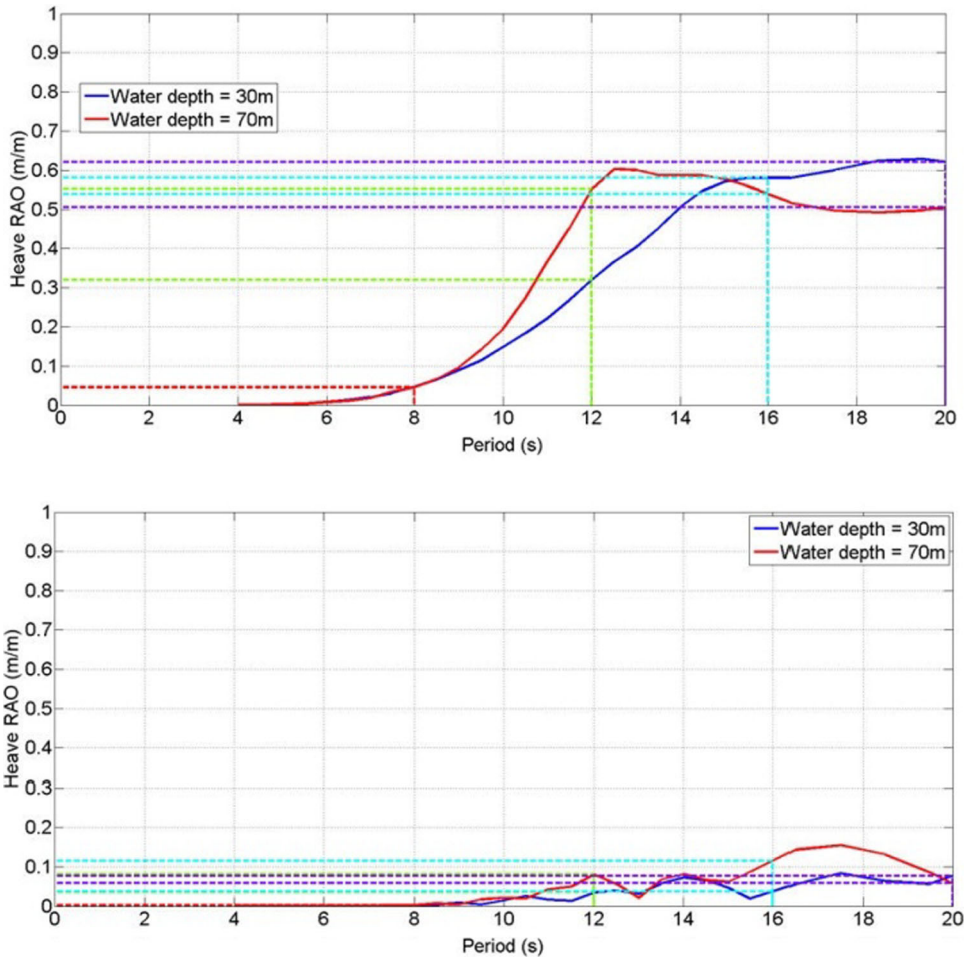

Fig. 25 Breakwater heave amplitude operator for several periods in 30 and 70 m water depth. Southward (*top*) and Northeast (*bottom*) wave incidence

structural model, as described earlier), KB is the vertical center of buoyancy ($T/2$), and $\mathrm{BM_{min}}$ is the ratio between the minimum waterline moment of inertia and the breakwater displacement volume.

$$\mathrm{GM_{0min}} = \mathrm{KB} + \mathrm{BM_{min}} - \mathrm{KG} \tag{18}$$

Since there is lack of symmetry in both x and y directions, the principal axis must be computed in order to evaluate the minimum moment of inertia, which is performed based on Mohr's circle Eq. (19), where I_{xx} and I_{yy} are the moments of inertia about the x and y axes with origin in the center of floatation of the breakwater and I_{xy} is the cross product of inertia, calculated from Eqs. (20), (21), and (22), respectively. The center of waterline area coordinates (x_{AWL}, y_{AWL}) are obtained from Eqs. (23) and (24), assuming a coordinate system with origin at the external corner of the "L" shape.

$$I_{\min} = \frac{I_{xx} + I_{yy}}{2} - \sqrt{\left(\frac{I_{xx} + I_{yy}}{2}\right)^2 - I_{xy}^2} \tag{19}$$

$$I_{xx} = \frac{bd^3}{12} + \left(y_{\mathrm{AWL}} - \frac{d}{2}\right)^2 bd + \frac{c(a-d)^3}{12} + c(a-d)\left(\frac{a+d}{2} - y_{\mathrm{AWL}}\right)^2 \tag{20}$$

$$I_{yy} = \frac{db^3}{12} + \left(\frac{b}{2} - x_{\mathrm{AWL}}\right)^2 bd + \frac{c^3(a-d)}{12} + c(a-d)\left(b - \frac{c}{2} - x_{\mathrm{AWL}}\right)^2 \tag{21}$$

$$I_{xy} = bd\left(\frac{b}{2} - x_{\mathrm{AWL}}\right)\left(\frac{d}{2} - y_{\mathrm{AWL}}\right) + c(a-d)\left(\frac{a+d}{2} - y_{\mathrm{AWL}}\right)\left(b - \frac{c}{2} - x_{\mathrm{AWL}}\right) \tag{22}$$

$$x_{\mathrm{AWL}} = \frac{\frac{b^2 d}{2} + \left(b - \frac{c}{2}\right)(a-d)c}{bd + (a-d)c} \tag{23}$$

$$y_{\mathrm{AWL}} = \frac{\frac{bd^2}{2} + \left(\frac{a+d}{2}\right)(a-d)c}{bd + (a-d)c} \tag{24}$$

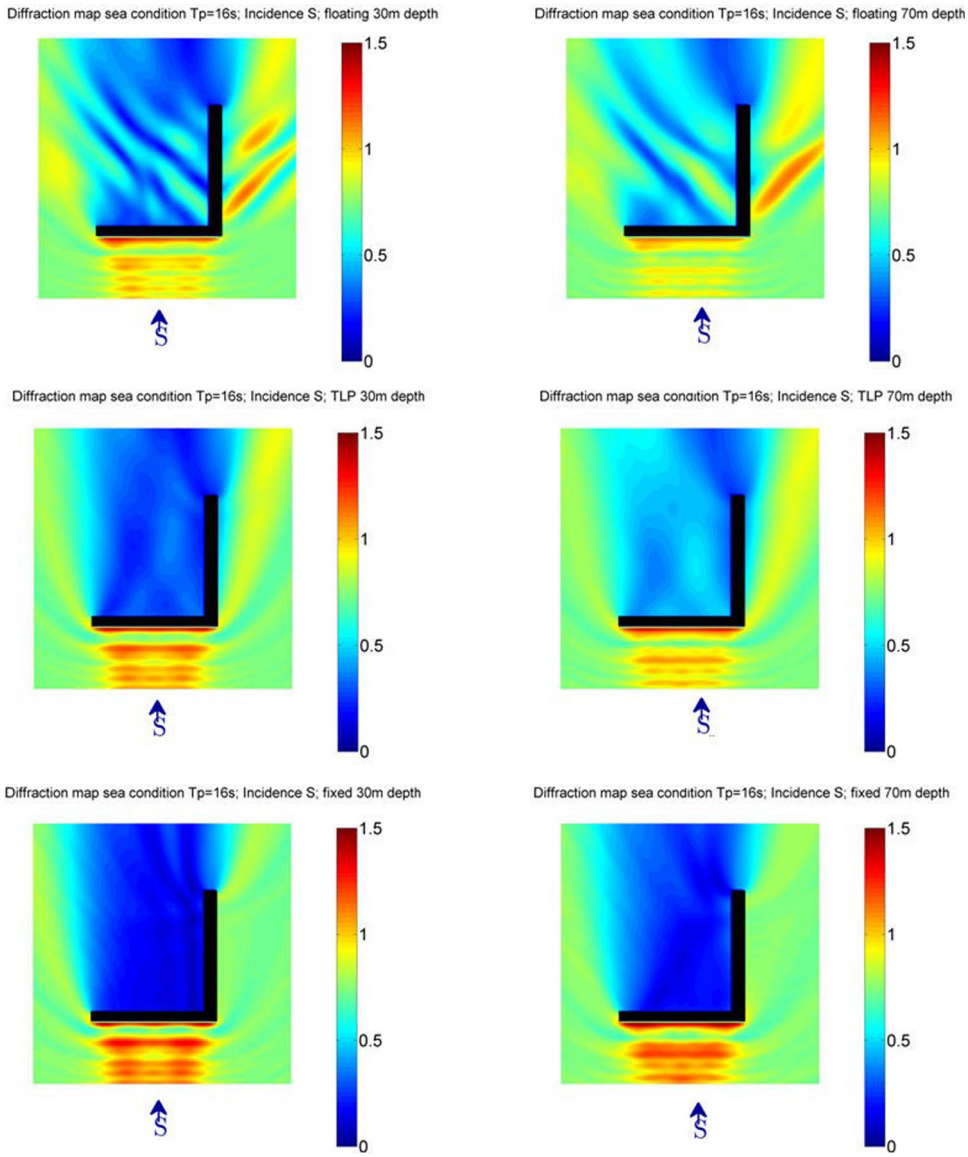

Fig. 26 Comparison between floating (*top*), TLP (*medium*) and fixed (*bottom*) breakwaters for 30 m water depth (*left*) and 70 m (*right*) sea condition. $T_p = 16$ s; southward wave incidence direction

Table 4 Design variable range for the floating breakwater

Design variable	Lower bound (m)	Upper bound (m)
a	600.0	1400.0
b	850.0	910.0
c	20.0	80.0
d	20.0	80.0
T	20.0	35.0

The results considering several variable combination in the range shown in Table 4 can be seen in Fig. 27, which presents the vertical center of buoyancy, vertical center of gravity (computed in the structural model), BM, and GM_{min}. It can be verified that the minimum metacentric height achieved is 100 m, illustrating that the stability is not a big issue for this type of structure.

6 Conclusions

This paper presented a parametric study of floating breakwaters focusing on the evaluation of its performance in terms of wave attenuation capability, seakeeping behavior, stability, structural feasibility, and cost estimation of breakwater fabrication in Brazil.

The analyses were performed considering a L-shaped floating breakwater structure subjected to different wave periods, directions, water depths, and rigid motions. The results illustrated that the wave attenuation capability is directly related to the wave period, in such a way that the wave elevation on the sheltered area tends to increase as

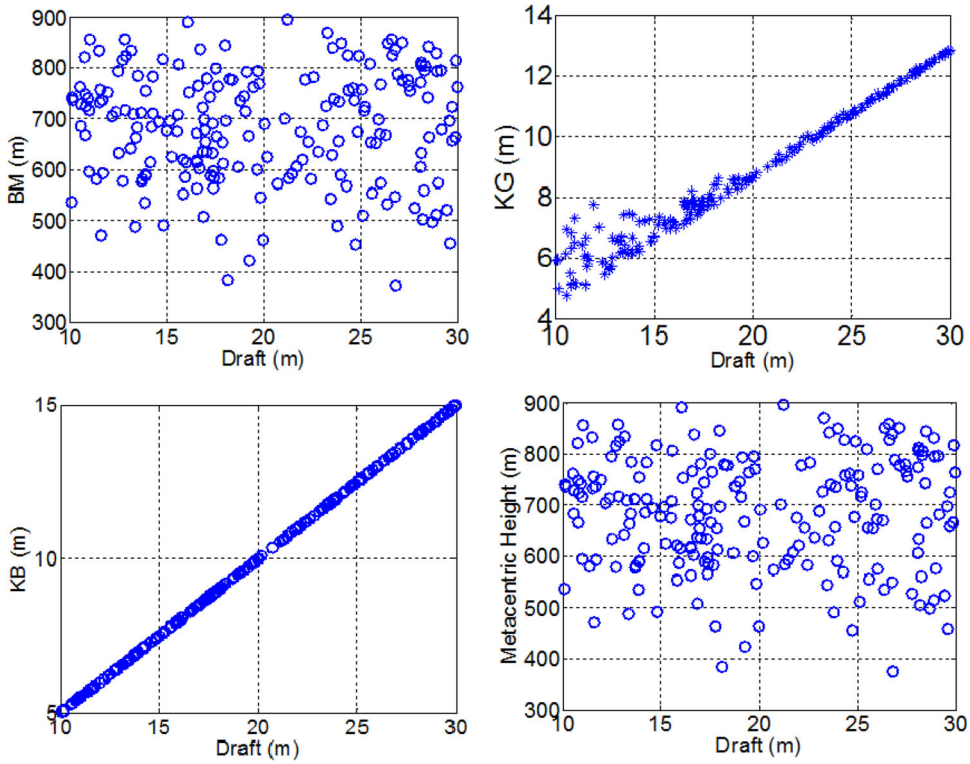

Fig. 27 BM, KG, KB, and GM_{0min} values for several floating breakwater configurations

the wave periods become larger. This is explained by the fact that the floating structure tends to reflect the propagation of the shortest waves almost completely, whereas the longest waves get around and pass beneath the body. In addition, the results also indicated that the motions of the floating body contribute significantly to the amplitude of waves downstream the breakwater structure. Indeed, the reduction in the floating breakwater motions also reduce the wave heights downstream the structure, this being an important aspect for the design of stiffer mooring systems to restrict the body motions.

Regarding the floating body stability, it was verified that the metacentric heights are high enough to ensure good stability. Therefore, stability is not an issue for this type of L-shaped structure.

The structural analysis was performed considering a simplified model to estimate the global strength (shear forces, bending moment, and torsion moment for critical wave conditions) as well as the body center of gravity and moment of inertia, which are important parameters for the motion analysis of the structure in waves. The loads are computed and the structural scantlings were increased accordingly to meet the strength requirements. Special attention is paid to the beam over draft ratio of the concrete structure to ensure the feasibility of the breakwater from a weight and floatation stand point.

Finally, this work indicated that a floating breakwater seems to be a cost-effective alternative to fixed structures in short period wave sites.

Acknowledgements The authors gratefully acknowledge BG Group for sponsoring this research and ANP (Brazil's National Oil, Natural Gas and Biofuels Agency) for the strategic importance of the support given through the R&D levy regulation. The authors also thanks the engineers Rafael M. Ribeiro, Thiago Peternella Rocha, and Rodrigo A. Schiller for the expert technical advice provided during this research.

References

1. A. Andrianov, Hydroelastic analysis of very large floating structures. PhD Thesis, TU Delft, 2005
2. A.C. Biesheuvel, Effectiveness of floating breakwaters: wave attenuating floating breakwaters. Master Thesis, TU Delft, 2013
3. DNV, DNV-OS-C502—offshore concrete structures. DET NORSKE VERITAS AS, 2012
4. M.W. Fousert, Floating breakwater: theoretical study of a dynamic wave attenuating system. Master Thesis, TU Delft, 2007
5. L.Z. Hales, Floating breakwaters: state-of-the-art literature review. Technical Report No. 81-1, U.S. Army, Corps of Engineers, Coastal Engineering Research Center, 1981
6. E. Koutandos, P. Prinos, X. Gironella, Floating breakwaters under regular and irregular wave forcing: reflection and transmission characteristics. J. Hydraulic Res. **43**, 174–188 (2005)
7. B.L. McCartney, Floating breakwater design. J. Waterway Port Coastal Ocean Eng. **111**(2), 304 (1985). 10.1061/(ASCE)0733-950X(1985)111:2(304)#sthash.2t7NdXZi.dpuf.
8. S. Miyajima, H. Seto, M. Ohta, Hydroelastic responses of the mega-float phase-II model in waves, in *Proceedings of the Twelfth (2002) International Offshore and Polar Engineering Conference*, 2002
9. PIANC, Harbour approach channels design guidelines, 2014.
10. PIANC, Floating breakwaters—a practical guide for design and construction. PTC2 report of WG 13, 1994

11. ROM 3.1-99, Recommendations for the design of the maritime configuration of ports, approach channels and harbour basins, 2007***
12. H. Saleh, Mega floating concrete bridges. Master Thesis, TU Delft, 2010
13. H. Suzuki, Overview of megafloat: concept, design criteria, analysis, and design. Mar. Struct. **18**, 111–132 (2005)
14. C. Valenchon, J.H. Rossig, S. Anrhs, Evolution of concrete monohulls after the Nkossa Barge, in *Offshore Technology Conference* (1997). doi:10.4043/8565-MS
15. WAMIT, User Manual Version 7.2 (2013). www.wamit.com